environmental microbiology

Environmental Microbiology (2017) **00**(00), 00–00 doi:10.1111/1462-2920.13980

Occurrence of chlorophyll allomers during virus-induced mortality and population decline in the ubiquitous picoeukaryote *Ostreococcus tauri*

Deborah J. Steele,[1,2] **Susan A. Kimmance**,[1] **Daniel J. Franklin**[2] **and Ruth L. Airs**[1]*

[1]*Plymouth Marine Laboratory, Prospect Place, Plymouth, UK.*

[2]*Faculty of Science and Technology, Bournemouth University, Poole, UK.*

Summary

During viral infection and growth limitation of the picoeukaryote *Ostreococcus tauri*, we examined the relationship between membrane permeability, oxidative stress and chlorophyll allomers (oxidation products). Chlorophyll allomers were measured in batch-cultures of *O. tauri* in parallel with maximum quantum efficiency of photosystem II photochemistry (F_v/F_m), carotenoids, and reactive oxygen species and membrane permeability using fluorescent probes (CM-H_2DCFDA and SYTOX-Green). Viral infection led to mass cell lysis of the *O. tauri* cells within 48 h. The concentration of the allomer hydroxychlorophyll *a* peaked with a 16-fold increase (relative to chlorophyll-*a*) just after the major lysis event. In contrast, cell death due to growth limitation resulted in a twofold increase in allomer production, relative to chl-*a*. Two allomers were detected solely in association with *O. tauri* debris after viral lysis, and unlike other allomers were not observed before viral lysis, or during cell death due to growth limitation. Conversely, the component chl-a_{P276} was found in the highest concentrations relative to chl-*a*, in exponentially growing *O. tauri*. The components described have potential as indicators of mode of phytoplankton mortality, and of population growth.

Introduction

Phytoplankton assemblages are highly variable in their functionality, and at times large proportions (up to 95%) can be classified as dead and non-photosynthetically functional (Veldhuis *et al.*, 2001; Agustí and Sánchez, 2002). It is generally assumed that intact pigment-containing cells are viable and therefore capable of manifesting physiological processes such as cell growth, repair and division, or that they are dormant. It is clear, however, that whole, non-functional and non-viable cells can be abundant and therefore contribute to ocean colour, and hence to estimates of chlorophyll *a* biomass. After phytoplankton death, caused by environmental factors such as nutrient depletion, temperature stress (Agustí *et al.*, 2006; Alonso-Laita and Agustí, 2006) or light stress (Berman-Frank *et al.*, 2004; Llabrés and Agustí, 2006; Llabrés *et al.*, 2010), intact but dead cells may persist. The chlorophyll contained in dead cells is not photosynthetically active, which could cause an uncoupling of estimates of chlorophyll *a* biomass and primary production (Key *et al.*, 2010). Therefore, it is essential to distinguish functional from non-functional phytoplankton cells.

Chlorophyll transformation i.e. alteration to the chlorophyll molecule, can arise from any disruption to the phytoplankton cell (Jeffrey and Vesk, 1997) via many different processes, and transformation products have been linked with different modes of phytoplankton mortality (Head and Horne, 1993; Walker and Keely, 2004; Bale *et al.*, 2011). The allomer (chlorophyll oxidation product) hydroxychlorophyll *a* (HO-chl-*a*) is thought to be common in phytoplankton during cell demise (Franklin *et al.*, 2012; Steele *et al.*, 2015) and is routinely detected during pigment analyses (Hooker *et al.*, 2005) if the HPLC method used is adequate for its detection, in both high density (Walker and Keely, 2004; Bale *et al.*, 2015; Steele *et al.*, 2015) and low density (Steele, 2014; Steele *et al.*, 2015) algal populations. Hydroxychlorophyll *a* has also been associated with the onset of bloom decline in naturally occurring phytoplankton populations (Walker and Keely, 2004; Steele *et al.*, 2015) and has been found to increase in sinking particles (dominated by diatom-derived material, Bale *et al.*, 2015). Chlorophyll allomers have also been assigned as markers of fresh photoautotrophic organic matter, originating from coastal zones with high dissolved oxygen (Szymczak-Żyła *et al.*, 2011). However, few studies have investigated phytoplankton cell physiological state and chl-*a* alterations (Franklin *et al.*, 2012).

Received 31 March, 2015; accepted 31 October, 2017. *For correspondence. E-mail RUAI@pml.ac.uk; Tel. +44 01752633100; Fax +44 (0)1752633101.

During cell death, when the mechanisms which protect the cell against oxidative stress break down, and/or programmed cell death (PCD) is induced, an increase in reactive oxygen species (ROS) inside the cell may increase the quantity of allomers relative to chlorophyll (Franklin *et al*., 2012). As HO-chl-*a* is the major product of chl-*a* in the presence of hydrogen peroxide, it is likely to be associated with conditions where peroxygens (e.g., hydrogen peroxide) are elevated (Walker *et al*., 2002), for example during oxidative stress. Intracellular ROS are by-products of regular cellular processes (e.g., photosynthesis) and are regulated by antioxidant mechanisms to avoid oxidative stress in the cell (Apel and Hirt, 2004). ROS are also known to be ubiquitous signalling molecules in the cells response to stress (Apel and Hirt, 2004; Halliwell, 2006; D'Autréaux and Toledano, 2007; Rosenwasser *et al*., 2014; Huang *et al*., 2016), and are known triggers of the PCD pathway (Bidle, 2015), which mediates cellular phytoplankton death processes, for example during cell death due to environmental factors; including dark-induced death of the chlorophyte *Dunaliella tertiolecta* (Segovia and Berges, 2009); and bloom-termination of the dinoflagellate *Peridinium gatunense* due to CO_2 limitation (Berman-Frank *et al*., 1994; Vardi *et al*., 1999). This induction of PCD by ROS also occurs during virus-induced cell death of *E. huxleyi* (Bidle *et al*., 2007; Vardi *et al*., 2012; Sheyn *et al*., 2016) where the enzymatic production of ROS appears to be stimulated by *E. huxleyi* virus infection (Sheyn *et al*., 2016).

Viral lysis is a quantitatively significant fate for phytoplankton (Proctor and Fuhrman, 1990; Suttle *et al*., 1990; Cottrell and Suttle, 1995; Brussaard *et al*., 1996). Viruses are thought to be responsible for causing the release of about a quarter of all photosynthetically fixed carbon through cell lysis (Fuhrman, 1999), thereby regulating phytoplankton community structure (Murray and Jackson, 1992), biomass production and population density (Bratbak *et al*., 1993; Vardi *et al*., 2012). Virus-mediated death of phytoplankton is known to lead to degradation of photosynthetic pigments (Llewellyn *et al*., 2007), but the timing and specific effect on chlorophyll *a* during infection and lysis are not well understood. Host photosynthesis is not always required for viral growth but varies with species (Benson and Martin, 1981; Van Etten *et al*., 1983; Suttle and Chan, 1993; Seaton *et al*., 1995; Juneau *et al*., 2003). Hence, the effect of viral infection on host photosynthetic capacity is variable. Pigment transformations during viral lysis of *Emiliania huxleyi* have been described (Llewellyn *et al*., 2007; Bale *et al*., 2013), and there is some evidence for production of chlorophyll allomers (Bale *et al*., 2013). These studies however, lack concurrent physiological measurements that describe the average phytoplankton population cell state during virus infection and lysis.

To assess the ubiquity of allomer formation and its potential co-occurrence with loss of algal cell function, it is important to expand the study of chlorophyll transformation during viral lysis beyond one genus. The cosmopolitan picoeukaryote *Ostreococcus tauri* was chosen for this study as it is an environmentally relevant primary producer for which a lytic virus has previously been isolated (thus, a model host:virus system was available, Derelle *et al*., 2008). Typically, picoeukaryotes are abundant in the world's oceans, have a relatively high rate of carbon fixation (Li, 1994; Worden *et al*., 2004) and are particularly important in the open ocean (Grob *et al*., 2011). Furthermore, the eukaryotic picoplankton genus *Ostreococcus* has a global distribution (coastal seas, the oligotrophic North Atlantic, the Mediterranean, the Indian and Pacific Oceans (Worden *et al*., 2004; Zhu *et al*., 2005; Countway and Caron, 2006), and a wide depth profile (surface waters to 120 m depth, Worden *et al*., 2004). Here we used a well characterised strain of *Ostrecoccus tauri* (OTH95 RCC745), which has undergone complete genomic sequencing (Derelle *et al*., 2006; Robbens *et al*., 2007), to analyse the relationship between cell demise and chlorophyll allomers.

This study describes the formation of chlorophyll allomers in *Ostreococcus tauri* during two mortality pathways: viral infection and growth limitation, with particular focus on the period directly before, and at the onset of, population decline. We performed concurrent measurements of *O. tauri* growth, OtV5 virus abundance, membrane permeability, cellular un-scavenged reactive oxygen species, chlorophyll *a* (chl-*a*), chlorophyll *b* (chl-*b*) and their allomers, the chl-*a* precursor (chl-a_{p276}), maximum quantum efficiency of photosystem II photochemistry (F_v/F_m), and the carotenoid components of the non-photochemical quenching xanthophyll cycle, to describe in detail the timing of allomer formation in relation to population physiological state.

Results

Virus-infected cultures; physiological indicators

The virus OtV5, which infects *O. tauri*, was added to triplicate *O. tauri* cultures after 3 days of growth. The observed cycle of infection was consistent with previous work by Derelle *et al*. (2008). Infected cultures began to decline between 8 and 24 hours post-infection (hpi, days 3.3 and 4, Fig. 1A). At this time the *O. tauri* population density and F_v/F_m decreased, while simultaneously SYTOX-Green staining for membrane permeability, increased (Fig. 1A–C). By 32 hpi (day 4.3), 93.4 $\pm$ 2.0% (mean $\pm$ SD) of the *O. tauri* population had lysed, and of the remaining cells, 52.5 $\pm$ 4.5% stained positively with SYTOX (Fig. 1C). The cytograms of *O. tauri* (Fig. 2) show cellular material which have retained a degree of red (chlorophyll-type)

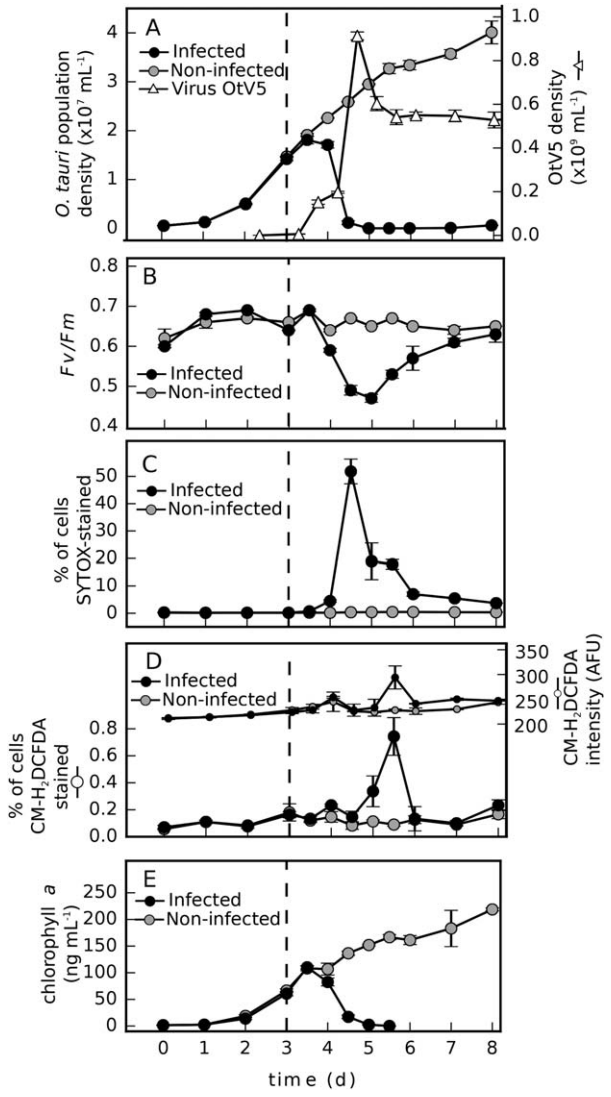

Fig. 1. Physiological response of *Ostreococcus tauri* OTH95 RCC745 infected with virus OtV5 and non-infected controls.
A. Population densities of *O. tauri*, and virus OtV5 particles.
B. Maximum quantum efficiency of PSII photochemistry (F_v/F_m).
C. Percentage of *O. tauri* cells stained with SYTOX-Green (for membrane permeability).
D. Percentage of cells stained with CM-H_2DCFDA (for intracellular reactive oxygen species), and mean fluorescence intensity.
E. Chlorophyll *a* content. Mean and SE bars shown ($n = 3$), - - - indicates time of OtV5 addition.

fluorescence (in the lower left hand corner). For flasks inoculated with OtV5, these cell fragments, labelled as debris, show maxima on days 5 and 5.3, just after the main lysis event between days 4 and 4.3 (Fig. 1A). This debris may have also contributed to the increased F_v/F_m values. In the control flasks, the relative proportion of cell debris remained relatively constant over the same period.

Virus numbers had increased (80 000-fold) by 8 hpi (day 3.3), however, the major viral lysis event occurred between 24 hpi (day 4) and 32 hpi (day 4.3). During this time OtV5 abundance peaked at 9×10^8 mL^{-1}. After viral inoculation CM-H_2DCFDA staining for detection of reactive oxygen species (ROS) was significantly elevated. The percentage of cells stained CM-H_2DCFDA-positive increased 0.6-fold relative to the non-inoculated control flasks 24 hpi (Fig. 1D, Mann-Whitney $U = 4.5$, $P < 0.05$). This CM-H_2DCFDA staining increased significantly (Spearman rank; $R = 0.714$, $P < 0.05$) over time in inoculated cultures to a maximum of 0.75 ± 0.14%, (a 7.3-fold increase) 56 hpi (day 5.3). Notably, the CM-H_2DCFDA stain was indicating non-scavenged ROS within intact *O. tauri* cells, i.e. those which had not lysed. A small residual surviving population of *O. tauri* began to regrow between 48 hpi and 56 hpi (days 5 and 5.3, Fig. 2), as identified previously in this *O. tauri* strain (Thomas *et al.*, 2011), with the specific growth rate (μ) of 0.07 ± 0.01 h^{-1}. This residual population was potentially resistant to infection by OTV5, and continued growing exponentially ($\mu \geq 0.69$) for at least 5 days. This residual population may account for the recovering photosynthetic capacity evident from F_v/F_m values (Fig. 1B).

*Virus-infected cultures; chlorophylls, allomers and chl-*a *precursor*

For chemical assignment of components, see below. All chlorophyll allomers reached their maximum concentration relative to their parent chlorophylls on day 5 (Fig. 3B–G), coinciding with the maximum proportion of cell debris observed in the cytograms (Fig. 2). The ratio of hydroxychlorophyll *b* (HO-chl-*b*) increased relative to chl-*b* above levels of the control flasks 24 hpi (day 4, 0.076 ± 0.003, mean $\pm$ SE, 0.9-fold increase), and reached a maximum of 0.42 ± 0.04 at 48 hpi (day 5, Fig. 3B, 9.9-fold increase. This timing of chl-*b* allomer production was matched by the dominant chl-*a* allomer produced during OtV5-infection, hydroxychlorophyll *a* (HO-chl-*a*) and its epimer. These HO-chl-*a* allomers, relative to chl-*a*, increased above levels of the control flasks 24 hpi, and reached their maxima of 0.110 ± 0.008 and 0.08 ± 0.009 respectively (equal to 26-fold and 78-fold increases) at 48 hpi (day 5, Fig. 3F and G), when 99.0 ± 2.8% of the *O. tauri* population had lysed. At this time, non-infected cultures maintained low levels of HO-chl-*a* of 0.004 ± 0.000.

After the major lysis event between 32 and 48 hpi, pigment samples contained methoxychlorophyll *a*-like (MeO-chl-*a*-like) and hydroxychlorophyll *a*-like (HO-chl-*a*-like) allomers, with average allomer to chl-*a* ratios of 0.015 ± 0.003 and 0.011 ± 0.002 respectively ($n = 6$, Fig. 3D and E). Unlike the other allomers, these components were not detected in the cultures before viral lysis, nor were they detected in the control cultures. The timing of the detection of methoxychlorophyll *a*-like and hydroxychlorophyll *a*-like coincided with high levels of cell debris

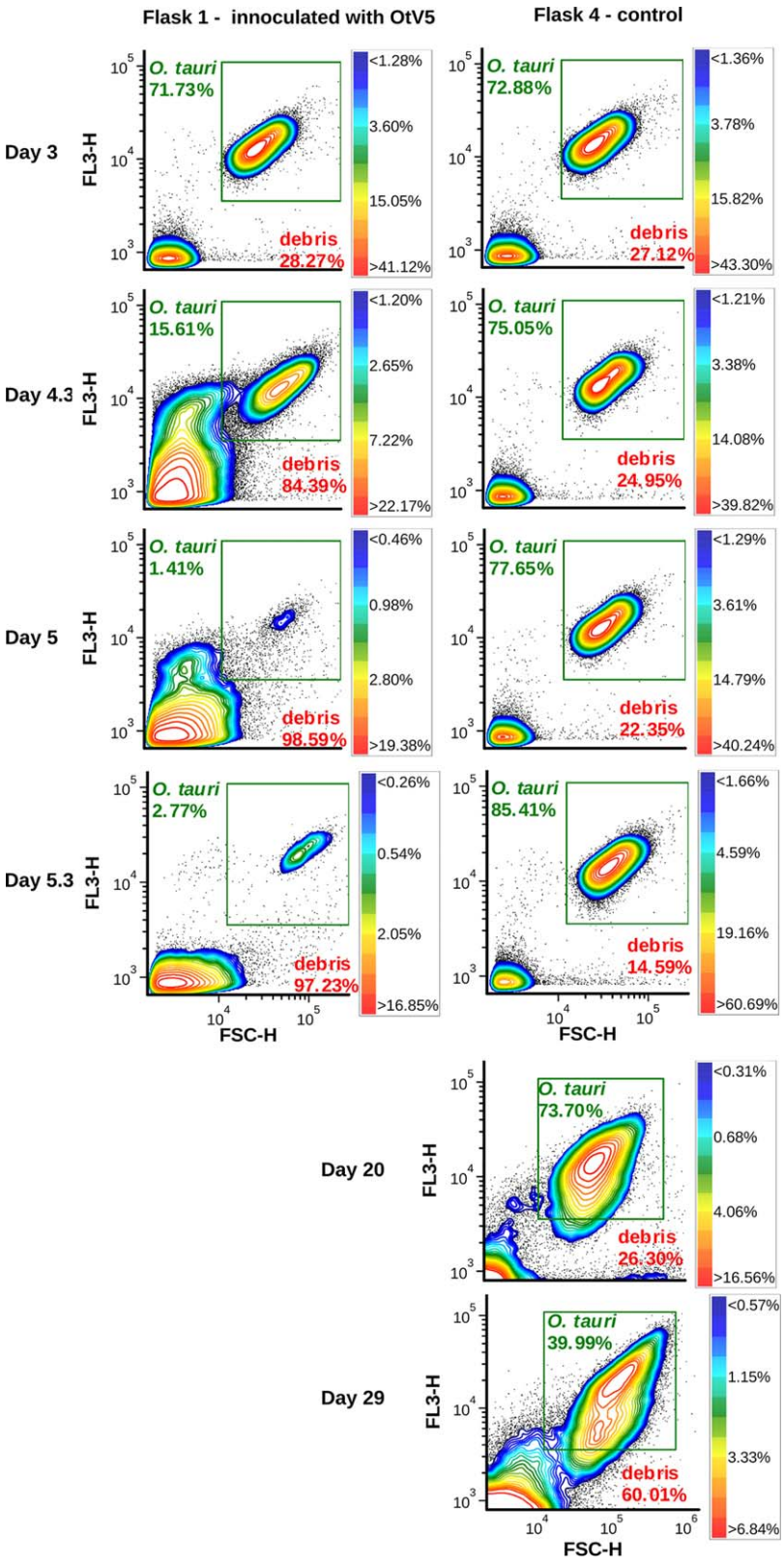

Fig. 2. Cytograms of an *Ostreococcus tauri* OTH95 RCC745 population during death by OtV5 lysis and re-growth of residual population (left column), and death by environmental limitation (right column). Population density plots representing all events acquired with red fluorescence: FL3-H (red fluorescence) and FSC-H (forward scatter).

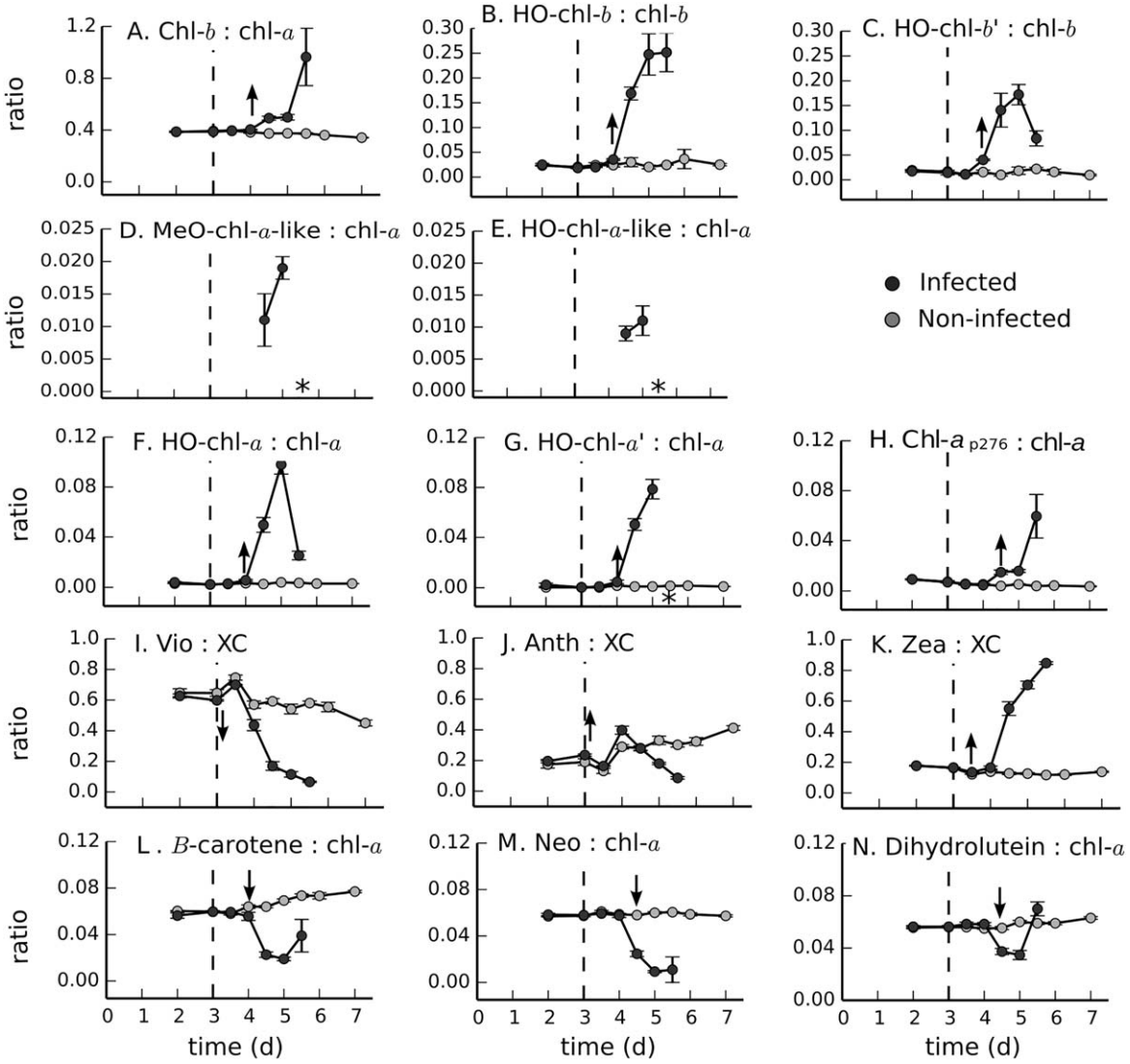

Fig. 3. Cellular chlorophyll, allomer and xanthophyll ratios in OtV5-infected and non-infected *O. tauri* cultures. Including ratios of: (A) chl-*b* to chl-*a*; the chl-*b* allomers (B) hydroxychlorophyll *b* and (C) epimer to chl-*b*; the chlorophyll *a* allomers (D) methoxychlorophyll-*a*-like allomer, (E) HO-chl-*a*-like allomer, (F) hydroxychlorophyll *a* and (G) epimer, to chl-*a*; (H) the chl-*a* precursor chl-a_{P276} to chl-*a*. Ratios of the xanthophylls: (I) Violaxanthin, (J) Antheraxanthin, and (K) Zeaxanthin, to the xanthophyll components (XC, Violaxanthin + Antheraxanthin + Zeaxanthin); and (L) Beta-carotene, (M) Neoxanthin, and (N) Lutin, to chl-*a*. Dashed line indicates time of virus addition. * indicates where quantification was not possible due to low biomass. ↑ indicates the first significant difference between OtV5-infected and non-infected cultures. Mean and SE bars shown ($n = 3$).

that showed high red fluorescence in the cytograms (days 4.3 and 5, Fig. 2).

Both chlorophyll *b*, and the chlorophyll *a* precursor chl-a_{P276} showed similar profiles relative to chl-*a* in the infected cultures (Fig. 3A and H). Both components showed small relative increases on days 4.3 and 5, and maximum abundance relative to chl-*a* on day 5.3 (Fig. 3A and H), coincident with the regrowth of the residual *O. tauri* population (Fig. 2). Chl-a_{P276} is a precursor in chlorophyll *a* biosynthesis, and chlorophyll *b* is used as a light harvesting chlorophyll in the peripheral antenna. Their small increases relative to chlorophyll *a* on day 4.3, during the main lysis event, may be due to their location in the peripheral antenna, whereas chlorophyll *a* is located in the core antenna and reaction centre as well as the peripheral antenna (Scheer, 2006) and therefore could be subject to a different rate of destruction during cell lysis.

Virus-infected cultures; carotenoids

In *O. tauri* (as well as higher plants and green-algae) the xanthophyll cycle consists of the conversion of violaxanthin to zeaxanthin via antheraxanthin. During viral infection and lysis, zeaxanthin increased relative to the total abundance

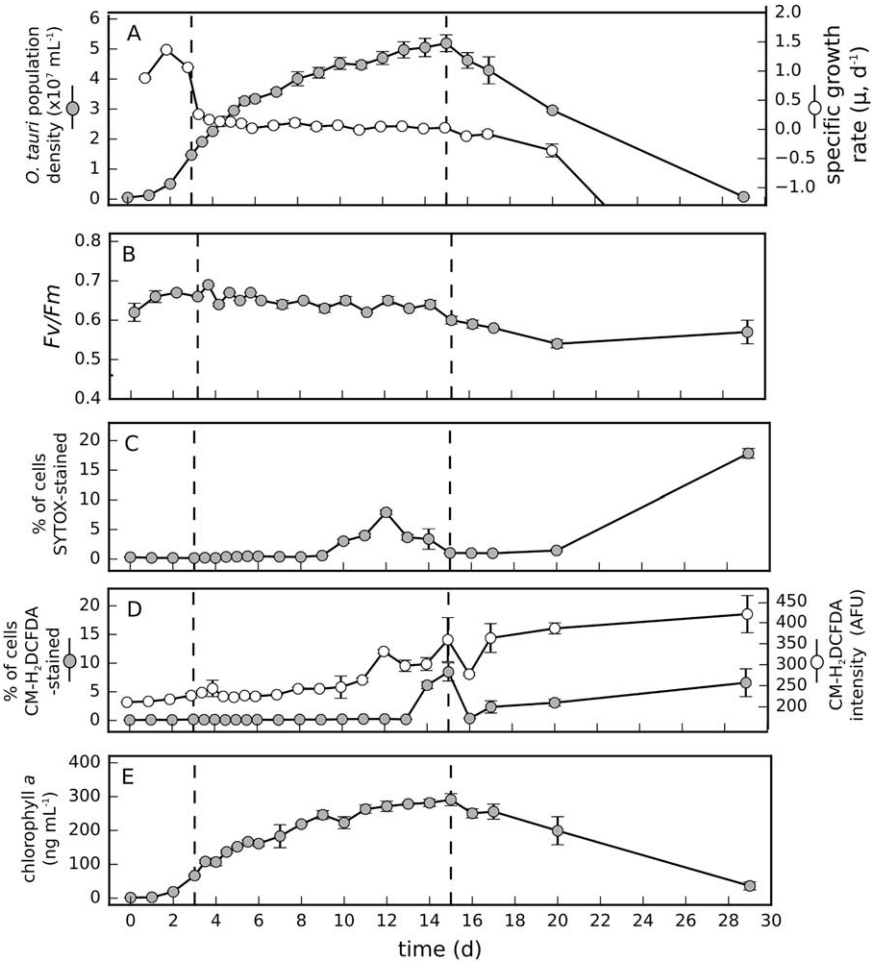

Fig. 4. Physiological changes of *Ostreococcus tauri* OTH95 RCC745 during batch culture growth, stationary and death phases (indicated by dashed lines). Including (A) Population density and specific growth rate (μ, d^{-1}) of *O. tauri*; (B) maximum quantum efficiency of PSII photochemistry (F_v/F_m); (C) Percentage of *O. tauri* cells stained with SYTOX-Green (for membrane permeability), (D) Percentage of *O. tauri* cells stained with CM-H_2DCFDA (for reactive oxygen species), and mean fluorescence intensity, (E) chlorophyll *a* content per cell. Mean and SE bars shown ($n = 3$).

of the xanthophyll cycle components, 24 hpi to 48 hpi (day 4–5, Fig. 3K). This coincided with a decrease in violaxanthin relative to the xanthophyll cycle pigments over the same period (Fig. 3I), indicating active conversion of violaxanthin to zeaxanthin during and after viral lysis. β-carotene, neoxanthin and dihydrolutein all decreased relative to chl-*a* between 24 hpi and 48 hpi (day 4 and day 5, Fig. 3L–N), and β-carotene and dihydrolutein then increased relative to chl-*a* at day 5.3, coincident with population regrowth.

Growth limited cultures; physiological indicators

Prior to the study, the *O. tauri* cultures were closely monitored and maintained in semi-continuous batch culture conditions with specific growth rate (μ) between 0.3 and 0.7 d^{-1}. The non OtV5-infected control populations of *O. tauri* were kept incubated under standard growth conditions and progressed through a typical batch culture cycle. These populations began to decline after 16 day of growth, most likely due to nutrient limitation, although nutrients were not directly measured (Fig. 4A). Assuming cells were using nutrients in the Redfield ratio; by calculation, phosphate was potentially the initial nutrient to become limiting, as F/2 media has an N:P ratio of 24:1. The concentration of chl-*a* increased throughout the stationary phase (days 3–15, Fig. 4E), then declined in line with the *O. tauri* population between days 15 and 29. F_v/F_m, a measurement of PSII photosynthetic efficiency, declined gradually after the population growth rate slowed (day 6, Fig. 4B), and further after 15 day, as the *O. tauri* population declined. SYTOX staining, indicating the proportion of cells with permeable membranes, increased from day 10 and peaked on day 12 (with $8.2 \pm 0.3\%$ of the population stained with SYTOX, a 24-fold increase), before declining (Fig. 4C). CM-H_2DCFDA staining (Fig. 4D), indicating the relative amount of reactive oxygen species within the cells, peaked at the onset of population density decline (day 15), to a maximum of $8.5 \pm 1.6\%$ (a 65-fold increase). After the onset of population decline (day 16) CM-H_2DCFDA and SYTOX staining increased again (from days 17 and 20 respectively) as cell physiological state further deteriorated.

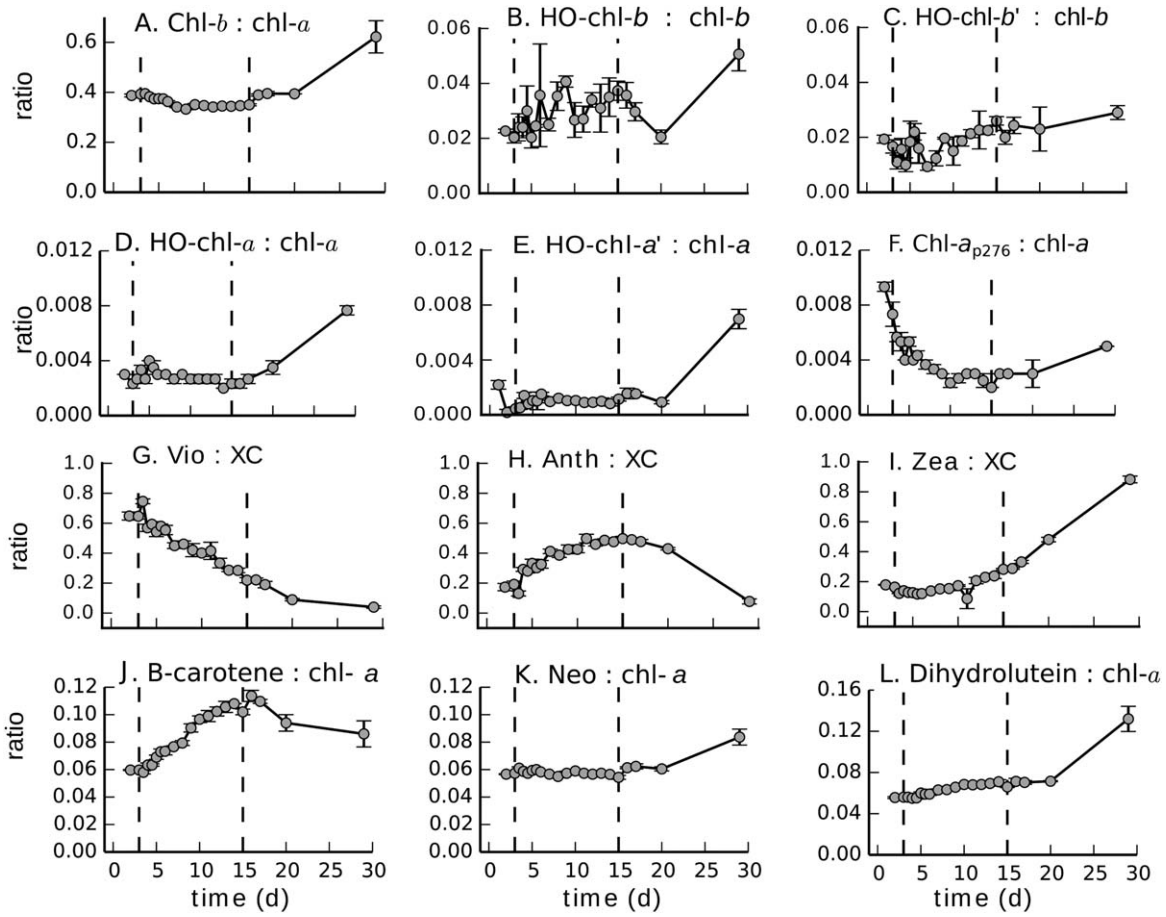

Fig. 5. Cellular chlorophyll, allomer and xanthophyll ratios in *Ostreococcus tauri* batch cultures. Including ratios of: (A) chl-*b* to chl-*a*; the chl-*b* allomers (B) hydroxychlorophyll *b* and (C) epimer, to chl-*b*; the chlorophyll *a* allomers (D) hydroxychlorophyll *a* and (E) epimer, to chl-*a*; (F) the chl-*a* precursor chl-a_{P276} to chl-*a*. Ratios of the xanthophylls: (G) Violaxanthin, (H) Antheraxanthin, (I) Zeaxanthin, to the xanthophyll components (XC, Violaxanthin + Antheraxanthin + Zeaxanthin) and (J) Beta-carotene, (K) Neoxanthin, and (L) Dihydrolutein, to chl-*a*. Batch culture growth, stationary and death phases are indicated by dashed lines. Mean and SE bars shown ($n = 3$).

*Growth limited cultures; chlorophylls, allomers and chl-*a *precursor*

All allomers showed increases relative to their parent chlorophyll during the death phase, between days 20 and 29 (Fig. 5B–E). The HO-chl-*b* to chl-*b* ratio increased during the death phase to a maximum of 0.075 ± 0.013 on day 29 (Fig. 5B and C, a 1.1-fold increase relative to day 5). HO-chl-*a* and HO-chl-*a*′ reached maxima of 0.0074 ± 0.0005 and 0.0072 ± 0.0007 (increases of twofold and sevenfold respectively from day 5, Fig. 5D and E). These increases were small compared to maximum levels observed after viral infection.

Chlorophyll *b* also increased during the death phase (Fig. 5A), and also reached a lower maximum than that observed after viral infection.

The component chl-a_{P276} was found in the highest concentration, relative to chl-*a*, in exponentially growing *O. tauri*, (days 0–3, when $\mu \geq 0.69$, Fig. 5F), consistent with its assignment as a precursor to chl-*a*. Like chlorophyll *b*, it also increased relative to chl-*a* between days 20 and 29.

Growth-limited cultures; carotenoids

Throughout the stationary and death phases the conversion of violaxanthin to zeaxanthin is evident (Fig. 5G–I). Notably, the maximum ratios of zeaxanthin to xanthophyll cycle components were similar for both fate processes (Fig. 3K and Fig. 5I). β-carotene increased (relative to chl-*a*) during the stationary phase, but decreased during the death phase (Fig. 5K). Conversely, neoxanthin and dihydrolutein increased relative to chl-*a* during the death phase (Fig. 5K and L).

Photosynthetic pigments; chemical assignment

Pigment extracts from OtV5-infected *Ostreococcus tauri* cultures and non-infected cultures were analysed for

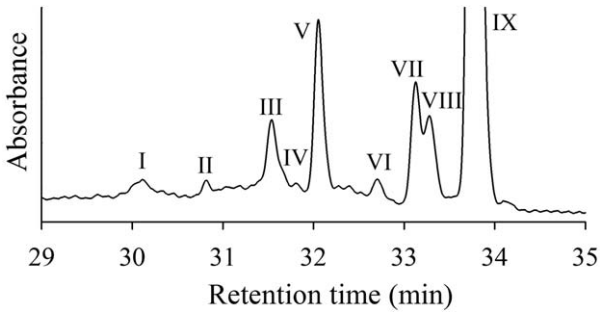

Fig. 6. Partial HPLC-PDA chromatogram (660 nm) of chlorophyll allomers detected in OtV5-infected O. *tauri* cultures 48 h post-infection (day 5), showing elution position relative to chl-*a* (IX) and chl-*b* (V). For peak assignment see Table 1.

Table 1. Main UV/vis absorption bands and assignment of components in Fig. 6.

Peak no.	Main UV/vis absorption bands (nm)	Assignment
I	427, (462), 653	Methoxychlorophyll *a*-like allomer
II	430, 481, 658	Hydroxychlorophyll *a*-like allomer
III	430, 660	Hydroxychlorophyll *b*
IV	430, 660	Hydroxychlorophyll *b*′
V	460, 648	Chlorophyll *b*
VI	430, 663	Chlorophyll a_{P276}
VII	420, 663	Hydroxychlorophyll *a*
VIII	430, 663	Hydroxychlorophyll *a*
IX	430, 663	Chlorophyll *a*

chlorophyll alteration products (Fig. 6). Assignments of chlorophyll *a* and chlorophyll *b* were made by comparison of their retention times to standards, comparison of UV/vis absorption spectra (Table 1) and major ions observed during LC/MS^n analysis (Table 2), to published data (Airs *et al*., 2001; Bale *et al*., 2011; Franklin *et al*., 2012). The extracts gave rise to several peaks which eluted in the region expected for chlorophyll allomers (Walker *et al*., 2002), prior to chlorophyll *a* (peak IX, Fig. 6), with UV/vis absorption spectra (Table 1) consistent with chl-*a* allomers (Franklin *et al*., 2012). An array of peaks exhibiting chlorin-like UV/vis spectra were also detected eluting prior to chl-*b* (Peak V, Fig. 6).

Peak I was present only in pigment extracts from the OtV5-infected cultures; it was not detected at any time in the non-infected cultures. During LC/MS/MS with post column addition of acid (Airs *et al*., 2001), peak I gave rise to precursor and daughter ions in the same pattern as methoxychlorophyll *a* (Table 2; Franklin *et al*., 2012), but with all components exhibiting an increased mass of 4 Da. The component is therefore assigned as methoxychlorophyll *a*-like allomer.

Peak II gave rise to a UV/vis absorption spectrum, as expected for a chl-*a* allomer but with an additional absorption band at 481 nm (Table 1). From LC/MS analysis with post-column acidification, peak II gave rise to one major ion at *m/z* 887 $[M + H\text{-}Mg]^+$. The MS^2 spectra contained a major ion at *m/z* 593 (Table 2), corresponding to a loss of 294 Da. Notably, the phytyl chain of chlorophylls *a* and *b* usually cleaves at the C—O bond with H^+ transfer to the charge retaining fragment during MS/MS resulting in the loss of the entire substituent with H^+ transfer (294 Da) instead of 278 Da. The mass of the entire phytyl constituent is, however 295 Da. It is possible therefore, that peak II was a chlorin esterified by phytol, but in such a stereochemical configuration to promote fragmentation via the loss of 294 Da instead of 278 Da. Notably, the MS^2 spectrum shows a less abundant ion at m/z 609, arising from the loss of 278 Da from the parent ion, providing support

Table 2. Abundant ions of peaks I-VII (see Fig. 6) observed during LC/MS/MS analysis of *O. tauri* pigment extracts.

		Peak no.							
Relationship to molecular ion	Structural assignment	I	II	III	IV	V	VI	VII	VIII
MH	$[M + H]^+$	927		923	923	907			909
MH-22	[M+H-Mg]+	905	887	901	901	885	869	887	887
MH-32	$[M+H\text{-}MeOH]^+$	873							
MH-32–278-60	$[M+H\text{-}MeOH\text{-}C_{20}H_{38}\text{-}CO_2Me]^+$	535							
MH-22–278	$[M+H\text{-}Mg\text{-}C_{20}H_{38}]^+$	627		623	623			609	609
MH-22–294	$[M+H\text{-}Mg\text{-}C_{20}H_{38}O]^+$		593						
MH-22–276	$[M+H\text{-}Mg\text{-}C_{20}H_{36}]^+$						593		
MH-22–278-60	$[M+H\text{-}Mg\text{-}C_{20}H_{38}\text{-}HCO_2Me]^+$	567							
MH-22–276-60	$[M+H\text{-}Mg\text{-}C_{20}H_{36}\text{-}HCO_2Me]^+$						533		
MH-22-18	$[M+H\text{-}Mg\text{-}H_2O]^+$			883	883				869
MH-22-18-278	$[M+H\text{-}Mg\text{-}H_2O\text{-}C_{20}H_{38}]^+$			605	605			591	591
MH-22–278-18–60	$[M+H\text{-}Mg\text{-}C_{20}H_{38}\text{-}H_2O\text{-}HCO_2Me]^+$							531	531
MH-22–294-18	$[M+H\text{-}Mg\text{-}\ C_{20}H_{38}O\text{-}H_20]^+$		575						
MH-278-60	$[M+H\text{-}C_{20}H_{38}\text{-}CO_2Me]^+$	589							
MH-278-32	$[M+H\text{-}C_{20}H_{38}\text{-}MeOH]^+$	617							

for the assignment of phytol as the esterifying alcohol, and indicating that both fragmentation mechanisms were taking place. It is important to note that the relative intensity of the ions in the MS^2 spectrum was low, and therefore the spectrum must be interpreted cautiously. Other fragmentations indicate the presence of a CO_2Me group (60 Da loss to produce an ion at *m/z* 533), and HO-substituent (18 Da loss to produce an ion at *m/z* 575), consistent with a hydroxychlorophyll *a* (HO-chl-*a*) structure. The component is therefore tentatively assigned as a hydroxychlorophyll *a*-type structure with unusual stereochemistry (HO-chl-*a*-like).

Peaks III and IV eluted in the region expected for chlorophyll *b* allomers, and were assigned as hydroxychlorophyll *b* and its epimer by comparison to published MS/MS data (Hyvärinen and Hynninen, 1999). Similarly, components VII and VIII were assigned as hydroxychlorophyll *a* and it's epimer based on MS^n data (Table 2; Walker *et al*. 2002).

Peak VI had a UV/vis absorption spectrum similar to chl-*a* (Airs *et al*., 2001) (Table 1). From LC/MS/MS with post-column addition of acid, peak VI gave rise to a major ion at *m/z* 869 corresponding to $[M + H\text{-}Mg]^+$ (Table 2). On resonance induced fragmentation, the ion at *m/z* 869, gave rise to *m/z* 593 in the MS^2 spectrum, equating to a loss of 276 Da indicating an extra double bond in the phytyl chain. The component at peak VI is therefore identified as a biosynthetic precursor to chlorophyll *a* (Rüdiger, 2006), chlorophyll a_{P276} (chl-a_{P276}). This component has been detected previously in *Thalassiosira pseudonana*, *Emiliania huxleyi* (Franklin *et al*., 2012) and *Pavlova gyrans* (Bale *et al*., 2011).

Discussion

Chlorophyll *a* allomers were produced in *Ostreococcus tauri* cultures 24 h post-infection (hpi) with OtV5, with an increase in the ratio of total chl-*a* allomers to chl-*a* of approximately 28-fold by 48 hpi (day 5). Allomers were also produced during *O. tauri* growth-limitation but in smaller amounts, with approximately a twofold increase in the ratio of total allomers to chl-*a*, 14 days after the onset of population decline. In flasks inoculated with OtV5, and in growth-limited flasks, the maximum ratio of allomers to chl-*a* coincided with the maximum proportion of cell debris detected in cytograms (day 5 and day 29 respectively, Fig. 2). Although the proportion of cell debris retained in the cell pellet during pigment sample collection via centrifugation is unknown, it can be assumed to be consistent between days 4.3 and 5.3, as the size spectrum of the debris, indicated by the forward scatter of the cytograms, did not change significantly during this period (Fig. 2). To be detected by flow cytometry (in this case), the cell debris must have exhibited red fluorescence, which arises from chlorophyll-type structures. Notably the debris showed maximum fluorescence on days 4.3 and 5 in samples from the infected flasks, and day 29 in the growth-limited flask (Fig. 2), coincident with the maximum increase in chlorophyll allomers relative to parent chlorophylls. The cell debris is likely to comprise a 'soup' of cellular components, including fragments of membrane and chloroplasts, and likely to be a prime source of reactive oxygen species, due to the presence of illuminated chlorophyll, and the disintegration of cellular machinery to prevent ROS formation and provide effective scavenging. Indeed, staining of the cell debris by CM-H_2DCFDA was observed, but not quantified (data not shown). Therefore, we propose that the increase in chlorophyll allomers observed after viral lysis and growth-limitation were formed in the cell debris, rather than in unlysed cells. Two allomers have been found solely in association with *O. tauri* lysis by OtV5; a methoxychlorophyll *a*-like allomer and a hydroxychlorophyll *a*-like allomer. These components were not detected prior to viral infection, or during growth limitation, and therefore may be specific to viral infection and lysis.

Measurement of ROS within the cells showed a response in OtV5-infected cultures—a 7.3-fold increase in the percentage of CM-H_2DCFDA-positive cells, but this was due to the small residual population. In the growth-limited population cellular ROS increased as growth limitation progressed, however, a peak in CM-H_2DCFDA-positive cells also occurred just prior to population decline (day 15). A peak in SYTOX-positive cells (with compromised membranes) occurred prior to this (day 12). Cell cycle arrest in a part of, or in the whole population during stationary phase may have allowed this build-up of ROS. A peak in ROS before population decline has also been detected in the diatom *Thalassiosira oceanica* (D. J. Steele, unpublished). The proportion of cells detected with compromised membranes during OtV5-infection was much greater (maximum 51.8%), although as the lysis process happens quickly, there was only a brief window when membranes were compromised but cells were still relatively intact. This level of SYTOX staining is comparable to that of natural picoplankton (Veldhuis *et al*., 2001; Baudoux *et al*., 2008), and small eukaryote (Veldhuis *et al*., 1997) populations in mixed natural assemblages, where between 3% and 75% of the cells stained SYTOX-positive.

It is possible that the retention of CM-H_2DCFDA was very poor in *O. tauri*, as only a small percentage of cells were stained (maximum 8.5%). Low levels of CM-H_2DCFDA staining have also been observed during viral infection of *Emiliania huxleyi* CCMP 1516 with mean probe intensity increasing 0.4-fold (approx) 48 hpi, up to twofold (approx.) 76 hpi (Evans *et al*., 2006); and in *E. huxleyi* CCMP 2090, where staining increased 0.5-fold (approx.) 72 hpi (Sheyn *et al*., 2016). Elevated intracellular ROS (up to 40% CM-H_2DCFDA-positive) was observed during the

late lytic phase of viral infection of a natural coccolithophore population (Vardi *et al*., 2012). The physiological differences in cell type between *E. huxleyi* (Prymnesiophyte) and *O. tauri* (Prasinophyte) may account for differences in CM-H_2DCFDA uptake. Even after careful optimisation and validation, probe response was limited in *O. tauri*. However, it appears that the cells capacity to buffer ROS, in particular hydroxyl radicals and peroxynitrite anions, which the probe is most sensitive to (Haugland, 2010), was maintained during OtV5-infection and growth-limitation via ROS scavenging and non-photochemical quenching.

The xanthophyll cycle dissipates excess excitation energy which would otherwise lead to the formation of destructive singlet oxygen ($^1O_{2)}$. The product of this xanthophyll cycle, zeaxanthin, deactivates excited singlet chlorophyll (Niyogi *et al*., 1998) and is also an antioxidant in the lipid phase of the thylakoid membrane (Havaux *et al*., 2007). The increase of zeaxanthin 24 hpi indicates that the xanthophyll cycle, a non-photochemical quenching (NPQ) process, increased in rate, during decreased photochemical quenching, reflected by decreased F_v/F_m 24 hpi (Fig. 1B). β-carotene is a precursor to the xanthophylls, and is also a ROS scavenger (Fiedor *et al*., 2001; 2005), specifically of $^1O_2$ (Telfer, 2002). β-carotene decreased relative to chl-*a* 24 hpi. As β-carotene is situated in the reaction centres (Young, 1993; Fiedor *et al*., 2001; 2005; Telfer, 2002), it also may be more prone to photooxidation (Llewellyn *et al*., 2007). Therefore, its decrease may be due to $^1O_2$ scavenging and photodegradation of the photosystem by ROS. This, along with the increased rate of non-photochemical quenching, prevented the build-up of cellular ROS, hence chlorophyll allomers remained low until after the major lysis events, due to OtV5-infection, and growth-limitation.

This capacity of *O. tauri* to buffer ROS accounts for the minimal chlorophyll allomer production of cultures before cell lysis. Increased formation of cellular HO-chl-*a* during cell lysis by viral action has been observed previously in *E. huxleyi* CCMP 1516 (Bale *et al*., 2013); an increase of approx. fourfold in absolute mass per cell, where the ratio of HO-chl-*a* to chl-*a* increased from approx. 0.004 at the beginning of population decline (4 days post-infection), increasing to approx. 0.02 after the loss of 94% of the population (16 days post-infection). Notably this also represents cellular HO-chl-*a* plus HO-chl-*a* in cell debris, which would have been collected by filtration. Here, hydroxychlorophyll *a* production in growth-limited *O. tauri* cultures, was consistent with previous observations during senescence of *Isochrysis galbana* (Prymnesiophyte, Bale *et al*., 2011) and *Thalassiosira pseudonana* (Diatom, Franklin *et al*., 2012). Chlorophyll *a* allomers have been observed not to increase during population decline of *E. huxleyi* (Franklin *et al*., 2012), however it was hypothesised by Franklin *et al*. (2012) that the *E. huxleyi* population, under N-limitation, may have undergone a physiological change, possibly in preparation for meiosis, rather than mortality (Franklin *et al*., 2012). Also *E. huxleyi* can maintain PSII repair through periods of nitrogen depletion (Loebl *et al*., 2010), limiting PSII photo-inactivation and ROS production (Holt *et al*., 2004; Key *et al*., 2010), which may decrease the formation of the oxidation product HO-chl-*a*. Rates of PSII repair are lower in *O. tauri* and lower still in *T. pseudonana* (Six *et al*., 2009; Key *et al*., 2010), which is reflected in the higher ratios of HO-chl-*a* to chl-*a* in *T. pseudonana* (Franklin *et al*., 2012) compared to *O. tauri*, during growth limitation.

To date, in the published studies of chlorophyll allomers in phytoplankton cultures, HO-chl-*a* has been detected ubiquitously across taxa (Bale *et al*., 2011; 2013; Franklin *et al*., 2012), but production during cell death varies with species and mode of death. Therefore, the total HO-chl-*a* in a mixed, natural population will vary according to community composition and the modes of mortality taking place. In natural phytoplankton populations the main causes of mortality are grazing (Walsh, 1983), viral lysis (Suttle *et al*., 1990; Brussaard, 2004) and senescence due to environmental factors (Walsh, 1983). The contribution of each of these factors varies greatly with season and region. HO-chl-*a* has been detected in various natural waters (Walker and Keely, 2004; Steele, 2014; Bale *et al*., 2015; Steele *et al*., 2015). Increased concentrations of HO-chl-*a* have been reported in sinking particles, i.e., during a diatom bloom terminated by nutrient-limitation (Bale *et al*., 2015), and after declines of various phytoplankton blooms in the Western English Channel, (Steele *et al*., 2015). Unfortunately, none of the reports of HO-chl-*a* in natural waters (to date) have included viral enumeration. In *O. tauri*, the total amount of allomers (relative to chl-*a*) varied depending on the mode of death, from $13.8 \pm 2.1\%$ during viral-infection to $3.1 \pm 0.8\%$ during growth limitation. Hence when a bulk measurement of total chlorophyll *a* is taken from a population dominated by *O. tauri*, the contribution to allomers of this total will be greatly increased if viral-infection is occurring.

Here, the observed cycle of infection and lysis of *O. tauri* by OtV5 within 2 days of the maximum population density, with rates of population decline from 0.06 d^{-1} (24 hpi) to 3.69 d^{-1} (48 hpi), was comparable to the decline of two consecutive *O. tauri*-like (picoalga resembling *O. tauri*) algal blooms in West Neck Bay (Maine). The *O. tauri*-like algal cells contained virus-like particles, but were also grazed by heterotrophic nanoflagellates (O'Kelly *et al*., 2003). The blooms had maximum population densities of 2×10^5 and 5×10^5 cells mL^{-1}, and collapsed within 4 days and 6 days respectively. Following the bloom declines, the population of *O. tauri*-like cells began to regrow. The longer decline period was probably due to a

lower maximum population density, lower density of viruses and competition between viruses and grazers. This time-frame of bloom termination by a combination of viral lysis and grazing has been recorded for other phytoplankton taxa, with similar lysis rates e.g. *Emiliania huxleyi* (Prymnesiophyte, Bratbak *et al*., 1993; 1995; Castberg *et al*., 2001; Vardi *et al*., 2012); *Micromonas* spp (Prasinophyte, Evans *et al*., 2003); and *Phaeocystis globosa* (Prymnesiophyte, Baudoux *et al*., 2006). If the different rates of cell mortality caused by grazing and viral lysis changed, favouring viral lysis, our study suggests that allomer production would increase. For example, if the *O. tauri*-like blooms observed by O'Kelly *et al*. (2003) had declined with the maximum rate observed here (3.69 d^{-1}), the populations would have declined by 97% within 24 h of the population maxima, and resulted in the production of chl-*a* allomers (HO-chl-*a* + HO-chl-*a'* + HO-chl-*a*-like- + MeO-chl-*a*-like) at a ratio of approx. 0.2 with chl-*a*. If a bulk measurement of chl-*a* were taken at this time, the total chl-*a* measurement coming from the *O. tauri* population, would consist of 20% allomers.

Given previous (Bale *et al*., 2011; Franklin *et al*., 2012) and present observations; elevated hydroxychlorophyll *a* levels should be considered an indicator of phytoplankton death. The occurrence of the methoxychlorophyll-*a*-like and hydroxychlorophyll *a*-like allomers during this study (present after viral lysis of *O. tauri*), provides evidence that these allomers occur during termination by viral lysis. The ratio of allomers and chl-*a* precursors can be used to determine if the dominant population at a particular location is growing or declining—providing physiological context.

Experimental procedures

Cultures and viral infection

Unialgal triplicate cultures of *Ostreococcus tauri* (OTH95 RCC745) were grown in 5 L conical flasks containing 1 L artificial seawater base media ESAW (Harrison and Berges, 2005) enriched with F/2 nutrients (Guillard and Ryther, 1962). Bacterial contamination was minimised by regular sub-culturing (every 3 days) prior to the study. Illumination from cool white fluorescent tubes was provided at 100 - 130 μmol photons m^{-2} s^{-1} on a 16: 8 h, light: dark cycle, at 20°C constant temperature. The populations were monitored daily, with samples taken at 9:00 h until virus addition, and twice daily thereafter (at 9:00 h and 17:00 h). Exponentially growing cultures ($\mu \geq 0.69$) were infected in triplicate with OtV5 lysate (Derelle *et al*., 2008) at a host to virus ratio of 1. Sampling of the OtV5-infected flasks ceased after the population had crashed. The non-infected control flasks were sampled daily until their population density began to decline (day 29), and formed the growth-limited study. The maximum quantum efficiency of PSII photochemistry (F_v/F_m; 15 min dark acclimation) was determined as soon as possible after sampling using a FIRe Fluorometer (Satlantic). Filtered, non-enriched ASW media (0.2 μm) was used as a blank and data was processed using FIRe-WORX software (Copyright 2007 Audrey B. Barnett).

Algal staining and enumeration

SYTOX-Green (Invitrogen S7020) used to measure changes in membrane permeability (Veldhuis *et al*., 1997); was applied at 0.5 μmol L^{-1} final concentration with incubation in the dark at 20°C for 15 min. CM-H_2DCFDA (5-and 6-chloromethyl-2′,7′-dichlorodihydrofluorescein diacetate, Invitrogen C6827), used to measure the relative amount of reactive oxygen species within a cell, was applied at 5 μmol L^{-1} final concentration (dark, 20°C for 30 min). Incubation conditions were optimised prior to the study using positive controls (Peperzak and Brussaard, 2011); for SYTOX, heat-killed cells (80°C, 5 min) and for CM-H_2DCFDA, hydrogen peroxide treated cells (10 μmol L^{-1} final concentration). Uptake of the stain was compared with unstained cells by flow cytometry, using an excitation laser of 488 nm, on a green (530/30 nm) versus red fluorescence (670 nm) plot. *O. tauri* population density was also quantified by flow cytometry (Accuri C6, BD Biosciences): Milli-Q was used as sheath fluid and analysis was triggered on forward scatter and red fluorescence. A core size of 22 μm was used and the event rate was kept below 1000 events s^{-1} to avoid coincidence; when necessary samples were diluted with filtered media (0.2 μm). Flow rate was set to 66 μL min^{-1} and measured daily by uptake of Milli-Q over 5 min (by mass).

Viral enumeration

Samples (1 mL) were fixed with glutaraldehyde (0.5% final concentration for 15 min at 4°C), flash frozen in liquid nitrogen and stored at −80°C until analysis. Defrosted samples were diluted in TE buffer (10 mM Tris HCL, 1 mM EDTA, pH = 8) and stained with SYBR Green-1 at a final concentration of 5×10^{-5} commercial stock (Invitrogen S7585) (Brussaard *et al*., 2000) and incubated for 10 min at 80°C, and then 5 mins at room temperature. Samples were run on a FACScan flow cytometer (Becton Dickinson) triggered on green fluorescence and set to 'low' flow (~20 μL min^{-1}) for 1 min, with event rates between 100 and 500 cells s^{-1}.

Photosynthetic pigments

The sample volume for photosynthetic pigments varied over the course of the study. For the OtV5 treatment flasks sample volumes were as follows: 50 mL on days 0, 1 and 2; 30 mL on day 3; 15 mL on days 3.3 and 4; 10 mL on day 4.3 and 7 mL thereafter. The same volumes were collected from the control flasks from day 0 to day 4, 15 mL was sampled from control flasks on day 4.3; and 50 mL from day 5 onwards until the termination of the study. The culture samples were centrifuged (at 5300 × g for 20 min at 8°C), and the pellet was flash frozen in liquid nitrogen and stored at −80°C until analysis. Exhaustive extraction of pigments used acetone (90% in Milli-Q) under dim light by sonication (at 40 W, Vibra Cell Probe; Sonics) for 40 s. The extract was clarified by centrifugation at 17,000 × g (Thermo Scientific). A 200 μL aliquot of extract was mixed with 80 μL water in the autosampler, and 25 μL of

this mix was injected onto the column. Reversed-phase high performance liquid chromatography (HPLC) was carried out using an Accela system (Thermo Scientific) with photodiode array detector, controlled using ChromQuest software. Chromatography was performed using a Waters Symmetry 3.5 μm C_8 column (2.1 × 150 mm) with pre-column of the same phase. Elution used a mobile phase gradient composed of methanol, acetonitrile, aqueous pyridine (0.25 mol L^{-1}) and acetone (all HPLC grade) at a flow rate of 0.2 mL min^{-1} (Method B in Zapata *et al.*, 2000). Assignment of chlorophyll allomers was carried out by LC/MS^n using an Agilent 1200 HPLC with photodiode array detector, coupled via an atmospheric pressure chemical ionization (APCI) source to an Agilent 6330 ion trap mass spectrometer. HPLC conditions were as described above with instrument control and analysis performed using Chemstation software. The following MS settings were used (positive ion mode): drying temperature 350°C, APCI vaporizer temperature 450°C, nebulizer 60 psi, drying gas 5 L min^{-1}, capillary voltage −4500 V, scan range *m/z* 400–1100. Formic acid was added to the HPLC elutant at 300 μL h^{-1} to aid ionisation (Airs and Keely, 2000). MS^n settings were used as follows: SPS on, number of precursor ions 2, isolation width 3 *m/z*.

Acknowledgements

We would like to thank Nigel Grimsley for providing the *O. tauri* OTH95 RCC745/OtV5, host/virus system. This work was supported by the Natural Environment Research Council [grant number NE/I528034/1].

References

Agustí, S., Alou, E.V.A., Hoyer, M.V., Frazer, T.K., and Canfield, D.E. (2006) Cell death in lake phytoplankton communities. *Freshw Biol* **51:** 1496–1506.

Agustí, S., and Sánchez, M.C. (2002) Cell viability in natural phytoplankton communities quantified by a membrane permeability probe. *Limnol Oceanogr* **47:** 818–828.

Airs, R.L., and Keely, B.J. (2000) A novel approach for sensitivity enhancement in atmospheric pressure chemical ionisation liquid chromatography/mass spectrometry of chlorophylls. *Rapid Commun Mass Spectrom* **14:** 125–128.

Airs, R.L., Atkinson, J.E., and Keely, B.J. (2001) Development and application of a high resolution liquid chromatographic method for the analysis of complex pigment distributions. *J Chromatogr A* **917:** 167–177.

Alonso-Laita, P., and Agustí, S. (2006) Contrasting patterns of phytoplankton viability in the subtropical NE Atlantic Ocean. *Aquat Microb Ecol* **43:** 67–78.

Apel, K., and Hirt, H. (2004) Reactive oxygen species: metabolism, oxidative stress, and signal transduction. *Annu Rev Plant Biol* **55:** 373–399.

Bale, N.J., Airs, R.L., and Llewellyn, C.A. (2011) Type I and Type II chlorophyll *a* transformation products associated with algal senescence. *Org Geochem* **42:** 451–464.

Bale, N.J., Airs, R.L., Kimmance, S.A., and Llewellyn, C.A. (2013) Transformation of chlorophyll *a* during viral infection of *Emiliania huxleyi*. *Aquat Microb Ecol* **69:** 205–210.

Bale, N.J., Airs, R.L., Martin, P., Lampitt, R.S., and Llewellyn, C.A. (2015) Chlorophyll-*a* transformations associated with sinking diatoms during termination of a North Atlantic spring bloom. *Mar Chem* **172:** 23–33.

Baudoux, A.-C., Noordeloos, A.A., Veldhuis, M.J., and Brussaard, C.P. (2006) Virally induced mortality of *Phaeocystis globosa* during two spring blooms in temperate coastal waters. *Aquat Microb Ecol* **44:** 207–217.

Baudoux, A.-C., Veldhuis, M.J.W., Noordeloos, A.A.M., Van Noort, G., and Brussaard, C.P.D. (2008) Estimates of virus vs. grazing induced mortality of picophytoplankton in the North Sea during summer. *Aquat Microb Ecol* **52:** 69–82.

Benson, R., and Martin, E. (1981) Effects of photosynthetic inhibitors and light-dark regimes on the replication of cyanophage SM-2. *Arch Microbiol* **129:** 165–167.

Berman-Frank, I., Zohary, T., Erez, J., and Dubinsky, Z. (1994) CO_2 availability, carbonic anhydrase, and the annual dinoflagellate bloom in Lake Kinneret. *Limnol Oceanogr* **39:** 1822–1834.

Berman-Frank, I., Bidle, K.D., Haramaty, L., and Falkowski, P.G. (2004) The demise of the marine cyanobacterium, *Trichodesmium* spp., via an autocatalyzed cell death pathway. *Limnol Oceanogr* **49:** 997–1005.

Bidle, K.D. (2015) The molecular ecophysiology of programmed cell death in marine phytoplankton. *Annu Rev Mar Sci* **7:** 341–375.

Bidle, K.D., Haramaty, L., e Ramos, J.B., and Falkowski, P. (2007) Viral activation and recruitment of metacaspases in the unicellular coccolithophore, *Emiliania huxleyi*. *Proc Natl Acad Sci USA* **104:** 6049–6054.

Bratbak, G., Egge, J.K., and Heldal, M. (1993) Viral mortality of the marine alga *Emiliania huxleyi* (Haptophyceae) and termination of algal blooms. *Mar Ecol Prog Ser* **93:** 39–48.

Bratbak, G., Levasseur, M., Michaud, S., Cantin, G., Fernandez, E., Heimdal, B.R., and Heldal, M. (1995) Viral activity in relation to *Emiliania huxleyi* blooms: a mechanism of DMSP release? *Mar Ecol Prog Ser* **128:** 133–142.

Brussaard, C.P. (2004) Viral control of phytoplankton populations—a review. *J Eukaryot Microbiol* **51:** 125–138.

Brussaard, C.P.D., Kempers, R.S., Kop, A.J., Riegman, R., and Heldal, M. and (1996) Virus-like particles in a summer bloom of *Emiliania huxleyi* in the North Sea. *Aquat Microb Ecol* **10:** 105–113.

Brussaard, C.P., Marie, D., and Bratbak, G. (2000) Flow cytometric detection of viruses. *J Virol Methods* **85:** 175–182.

Castberg, T., Larsen, A., Sandaa, R.A., Brussaard, C.P.D., Egge, J.K., and Heldal, M. (2001) Microbial population dynamics and diversity during a bloom of the marine coccolithophorid *Emiliania huxleyi* (Haptophyta). *Mar Ecol Prog Ser* **221:** 39–46.

Cottrell, M.T., and Suttle, C.A. (1995) Dynamics of lytic virus infecting the photosynthetic marine picoflagellate *Micromonas pusilla*. *Limnol Oceanogr* **40:** 730–739.

Countway, P.D., and Caron, D.A. (2006) Abundance and distribution of *Ostreococcus* sp. in the San Pedro Channel, California, as revealed by quantitative PCR. *Appl Environ Microbiol* **72:** 2496–2506.

D'Autréaux, B., and Toledano, M.B. (2007) ROS as signalling molecules: mechanisms that generate specificity in ROS homeostasis. *Nat Rev Mol Cell Biol* **8:** 813–824.

Derelle, E., Ferraz, C., Rombauts, S., Rouzé, P., Worden, A.Z., Robbens, S., *et al.* (2006) Genome analysis of the

smallest free-living eukaryote *Ostreococcus tauri* unveils many unique features. *Proc Natl Acad Sci USA* **103:** 11647–11652.

Derelle, E., Ferraz, C., Escande, M.-L., Eychenié, S., Cooke, R., and Piganeau, G. (2008) Life-cycle and genome of OtV5, a large DNA virus of the pelagic marine unicellular green alga *Ostreococcus tauri*. *PLoS One* **3:** e2250.

Evans, C., Archer, S.D., Jacquet, S., and Wilson, W.H. (2003) Direct estimates of the contribution of viral lysis and microzooplankton grazing to the decline of a *Micromonas* spp. population. *Aquat Microb Ecol* **30:** 207–219.

Evans, C., Malin, G., Mills, G.P., and Wilson, W.H. (2006) Viral Infection of *Emiliania huxleyi* (prymnesiophyceae) leads to elevated production of reactive oxygen species. *J Phycol* **42:** 1040–1047.

Fiedor, J., Fiedor, L., Winkler, J., Scherz, A., and Scheer, H. (2001) Photodynamics of the Bacteriochlorophyll–Carotenoid System. 1. Bacteriochlorophyll-photosensitized Oxygenation of β-Carotene in Acetone. *Photochem Photobiol* **74:** 64–71.

Fiedor, J., Fiedor, L., Haeßner, R., and Scheer, H. (2005) Cyclic endoperoxides of β-carotene, potential pro-oxidants, as products of chemical quenching of singlet oxygen. *Biochim Biophys Acta BBA - Bioenerg* **1709:** 1–4.

Franklin, D.J., Airs, R.L., Fernandes, M., Bell, T.G., Bongaerts, R.J., Berges, J.A., and Malin, G. (2012) Identification of senescence and death in *Emiliania huxleyi* and *Thalassiosira pseudonana*: Cell staining, chlorophyll alterations, and dimethylsulfoniopropionate (DMSP) metabolism. *Limnol Oceanogr* **57:** 305–317.

Fuhrman, J.A. (1999) Marine viruses and their biogeochemical and ecological effects. *Nature* **399:** 541–548.

Grob, C., Hartmann, M., Zubkov, M.V., and Scanlan, D.J. (2011) Invariable biomass-specific primary production of taxonomically discrete picoeukaryote groups across the Atlantic Ocean. *Environ Microbiol* **13:** 3266–3274.

Guillard, R.R., and Ryther, J.H. (1962) Studies of marine planktonic diatoms: I. *Cyclotella nana* Hustedt, and *Detonula confervacea* (CLEVE) Gran. *Can J Microbiol* **8:** 229–239.

Halliwell, B. (2006) Reactive species and antioxidants. Redox biology Is a fundamental theme of aerobic life. *Plant Physiol* **141:** 312–322.

Harrison, P.J., and Berges, J.A. (2005) Marine culture media. In *Algal Culturing Techniques*, Andersen, R. (ed.). Cambridge, MA, Academic Press, pp. 21–34.

Haugland, R.P. (2010) Probes for reactive oxygen species, including Nitric Oxide. In *Molecular Probes Handbook: A Guide of Fluorescent Probes and Labeling Technologies*. Spence, M.T. and Johnson, I.D. (eds). California, Life Technologies Corporation, pp. 483–503.

Havaux, M., Dall'osto, L., and Bassi, R. (2007) Zeaxanthin has enhanced antioxidant capacity with respect to all other xanthophylls in *Arabidopsis* leaves and functions independent of binding to PSII antennae. *Plant Physiol* **145:** 1506–1520.

Head, E.J.H., and Horne, E.P.W. (1993) Pigment transformation and vertical flux in an area of convergence in the North Atlantic. *Deep Sea Res Part II Top Stud Oceanogr* **40:** 329–346.

Holt, N.E., Fleming, G.R., and Niyogi, K.K. (2004) Toward an understanding of the mechanism of nonphotochemical quenching in green plants. *Biochemistry (Mosc)* **43:** 8281–8289.

Hooker, S.B., Van Heukelem, L., Thomas, C.S., Claustre, H., Ras, J., and Barlow, R. (2005) The second SeaWiFS HPLC analysis round-robin experiment (SeaHARRE-2). *NASA Tech Memo* **212785:** 124.

Huang, S., Aken, O.V., Schwarzländer, M., Belt, K., and Millar, A.H. (2016) The roles of mitochondrial reactive oxygen species in cellular signaling and stress response in plants. *Plant Physiol* **171:** 1551–1559.

Hyvärinen, K., and Hynninen, P.H. (1999) Liquid chromatographic separation and mass spectrometric identification of chlorophyll *b* allomers. *J Chromatogr A* **837:** 107–116.

Jeffrey, S.W., and Vesk, M. (1997) Introduction to marine phytoplankton and their pigment signatures. In *Phytoplankton Pigments in Oceanography: Guidelines to Modern Methods*. Jeffrey, S.W., Mantoura, R.F.C., Wright, S.W. (eds). Paris, UNESCO Publishing, pp. 37–84.

Juneau, P., Lawrence, J.E., Suttle, C.A., and Harrison, P.J. (2003) Effects of viral infection on photosynthetic processes in the bloom-forming alga *Heterosigma akashiwo*. *Aquat Microb Ecol* **31:** 9–17.

Key, T., McCarthy, A., Campbell, D.A., Six, C., Roy, S., and Finkel, Z.V. (2010) Cell size trade-offs govern light exploitation strategies in marine phytoplankton. *Environ Microbiol* **12:** 95–104.

Li, W.K. (1994) Primary production of prochlorophytes, cyanobacteria, and eukaryotic ultraphytoplankton: measurements from flow cytometric sorting. *Limnol Oceanogr* **39:** 169–175.

Llabrés, M., and Agustí, S. (2006) Picophytoplankton cell death induced by UV radiation: Evidence for oceanic Atlantic communities. *Limnol Oceanogr* **51:** 21–29.

Llabrés, M., Agustí, S., Alonso-Laita, P., and Herndl, G. (2010) *Synechococcus* and *Prochlorococcus* cell death induced by UV radiation and the penetration of lethal UVR in the Mediterranean Sea. *Mar Ecol Prog Ser* **399:** 27–37.

Llewellyn, C.A., Evans, C., Airs, R.L., Cook, I., Bale, N., and Wilson, W.H. (2007) The response of carotenoids and chlorophylls during virus infection of *Emiliania huxleyi* (Prymnesiophyceae). *J Exp Mar Biol Ecol* **344:** 101–112.

Loebl, M., Cockshutt, A.M., Campbell, D.A., and Finkel, A. Z V. (2010) Physiological basis for high resistance to photoinhibition under nitrogen depletion in *Emiliania huxleyi*. *Limnol Oceanogr* **55:** 2150–2160.

Murray, A.G., and Jackson, G.A. (1992) Viral dynamics: A model of the effects size, shape, motion and abundance of single-celled planktonic organisms and other particles. *Mar Ecol Prog Ser* **89:** 103–116. Oldendorf

Niyogi, K.K., Grossman, A.R., and Björkman, O. (1998) *Arabidopsis* mutants define a central role for the xanthophyll cycle in the regulation of photosynthetic energy conversion. *Plant Cell* **10:** 1121–1134.

O'Kelly, C.J., Sieracki, M.E., Thier, E.C., and Hobson, I.C. (2003) A transient bloom of *Ostreococcus* (Chlorophyta, Prasinophyceae) in West Neck Bay, Long Island, New York. *J Phycol* **39:** 850–854.

Peperzak, L., and Brussaard, C.P.D. (2011) Flow cytometric applicability of fluorescent vitality probes on phytoplankton. *J Phycol* **47:** 692–702.

Proctor, L.M., and Fuhrman, J.A. (1990) Viral mortality of marine bacteria and cyanobacteria. *Nature* **343:** 60–62.

Robbens, S., Derelle, E., Ferraz, C., Wuyts, J., Moreau, H., de Peer, Y.V. (2007) The complete chloroplast and mitochondrial DNA sequence of *Ostreococcus tauri*: Organelle genomes of the smallest eukaryote are examples of compaction. *Mol Biol Evol* **24:** 956–968.

Rosenwasser, S., Graff van Creveld, S., Schatz, D., Malitsky, S., Tzfadia, O., Aharoni, A., *et al*. (2014) Mapping the diatom redox-sensitive proteome provides insight into response to nitrogen stress in the marine environment. *Proc Natl Acad Sci USA* **111:** 2740–2745.

Rüdiger, W. (2006) Biosynthesis of chlorophylls *a* and *b*: the last steps. In *Chlorophylls and Bacteriochlorophylls*. Grimm, B., Porra, R.J., Rüdiger, W., and Scheer, H. (eds). Dordrecht, Springer, pp. 189–200.

Scheer, H. (2006) An overview of chlorophylls and bacteriochlorophylls: biochemistry, biophysics, functions and applications. In *Chlorophylls and Bacteriochlorophylls, Advances in Photosynthesis and Respiration*. Grimm, B., Porra, R.J., Rüdiger, W., and Scheer, H. (eds). Netherlands: Springer, pp. 1–26.

Seaton, G.G.R., Lee, K., and Rohozinski, J. (1995) Photosynthetic shutdown in *Chlorella* NC64A associated with the infection cycle of *Paramecium bursaria Chlorella* virus-1. *Plant Physiol* **108:** 1431–1438.

Segovia, M., and Berges, J.A. (2009) Inhibition of caspase-like activities prevents the appearance of reactive oxygen species and dark-induced apoptosis in the unicellular Chlorophyte *Dunaliella tertiolecta*. *J Phycol* **45:** 1116–1126.

Sheyn, U., Rosenwasser, S., Ben-Dor, S., Porat, Z., and Vardi, A. (2016) Modulation of host ROS metabolism is essential for viral infection of a bloom-forming coccolithophore in the ocean. *ISME J* **10:** 1642–1754.

Six, C., Sherrard, R., Lionard, M., Roy, S., and Campbell, D.A. (2009) Photosystem II and pigment dynamics among ecotypes of the green alga *Ostreococcus*. *Plant Physiol* **151:** 379–390.

Steele, D.J. (2014) Cellular viability and the occurrence and significance of chlorophyll allomers during phytoplankton turnover, PhD Thesis. Bournemouth University.

Steele, D.J., Tarran, G.A., Widdicombe, C.E., Woodward, E.M.S., Kimmance, S.A., Franklin, D.J., and Airs, R.L. (2015) Abundance of a chlorophyll *a* precursor and the oxidation product hydroxychlorophyll *a* during seasonal phytoplankton community progression in the Western English Channel. *Prog Oceanogr* **137:** 434–445.

Suttle, C.A., and Chan, A.M. (1993) Marine cyanophages infecting oceanic and coastal strains of *Synechococcus*: abundance, morphology, cross-infectivity and growth characteristics. *Mar Ecol-Prog Ser* **92:** 99–99.

Suttle, C.A., Chan, A.M., and Cottrell, M.T. (1990) Infection of phytoplankton by viruses and reduction of primary productivity. *Nature* **347:** 467–469.

Szymczak-Żyła, M., Kowalewska, G., and Louda, J.W. (2011) Chlorophyll *a* and derivatives in recent sediments as indicators of productivity and depositional conditions. *Mar Chem* **125:** 39–48.

Telfer, A. (2002) What is β–carotene doing in the photosystem II reaction centre? *Philos Trans R Soc Lond B Biol Sci* **357:** 1431–1440.

Thomas, R., Grimsley, N., Escande, M., Subirana, L., Derelle, E., and Moreau, H. (2011) Acquisition and maintenance of resistance to viruses in eukaryotic phytoplankton populations. *Environ Microbiol* **13:** 1412–1420.

Van Etten, J.L., Burbank, D.E., Xia, Y., and Meints, R.H. (1983) Growth cycle of a virus, PBCV-1, that infects *Chlorella*-like algae. *Virology* **126:** 117–125.

Vardi, A., Berman-Frank, I., Rozenberg, T., Hadas, O., Kaplan, A., and Levine, A. (1999) Programmed cell death of the dinoflagellate *Peridinium gatunense* is mediated by CO2 limitation and oxidative stress. *Curr Biol* **9:** 1061–1064.

Vardi, A., Haramaty, L., Van Mooy, B.A., Fredricks, H.F., Kimmance, S.A., Larsen, A., and Bidle, K.D. (2012) Host–virus dynamics and subcellular controls of cell fate in a natural coccolithophore population. *Proc Natl Acad Sci USA* **109:** 19327–19332.

Veldhuis, M.J., Cucci, T.L., and Sieracki, M.E. (1997) Cellular DNA Content of marine phytoplankton using two new fluorochromes: Taxonomic and ecological implications. *J Phycol* **33:** 527–541.

Veldhuis, MJ. W., Kraay, G.W., and Timmermans, K.R. (2001) Cell death in phytoplankton: correlation between changes in membrane permeability, photosynthetic activity, pigmentation and growth. *Eur J Phycol* **36:** 167–177.

Walker, J.S., Squier, A.H., Hodgson, D.A., and Keely, B.J. (2002) Origin and significance of 13 2-hydroxychlorophyll derivatives in sediments. *Org Geochem* **33:** 1667–1674.

Walker, J.S., and Keely, B.J. (2004) Distribution and significance of chlorophyll derivatives and oxidation products during the spring phytoplankton bloom in the Celtic Sea April 2002. *Org Geochem* **35:** 1289–1298.

Walsh, J.J. (1983) Death in the sea: enigmatic phytoplankton losses. *Prog Oceanogr* **12:** 1–86.

Worden, A.Z., Nolan, J.K., and Palenik, B. (2004) Assessing the dynamics and ecology of marine picophytoplankton: the importance of the eukaryotic component. *Limnol Oceanogr* **49:** 168–179.

Young, A.J. (1993) Factors that affect the carotenoid composition of higher plants and algae. In *Carotenoids in Photosynthesis*. Young, D.A.J. and Britton, D.G. (eds). Netherlands, Springer, pp. 160–205.

Zapata, M., Rodríguez, F., and Garrido, J.L. (2000) Separation of chlorophylls and carotenoids from marine phytoplankton: a new HPLC method using a reversed phase C8 column and pyridine-containing mobile phases. *Mar Ecol Prog Ser* **195:** 29–45.

Zhu, F., Massana, R., Not, F., Marie, D., and Vaulot, D. (2005) Mapping of picoeucaryotes in marine ecosystems with quantitative PCR of the 18S rRNA gene. *FEMS Microbiol Ecol* **52:** 79–92.